Manuscript prepared for Atmos. Chem. Phys.
with version 5.0 of the LaTeX class copernicus.cls.
Date: 22 July 2015

Turbulence vertical structure of the boundary layer during the afternoon transition

Clara Darbieu[1], Fabienne Lohou[1], Marie Lothon[1], Jordi Vilà-Guerau de Arellano[2], Fleur Couvreux[3], Pierre Durand[1], David Pino[4,5], Edward G. Patton[6], Erik Nilsson[1,7], Estel Blay-Carreras[4], and Beniamino Gioli[8]

[1]Laboratoire d'Aérologie, Toulouse, CNRS UMR 5560, Université de Toulouse, Toulouse, France
[2]Meteorology and Air Quality Section, Wageningen University, Wageningen, The Netherlands
[3]CNRM-GAME (Météo-France and CNRS), Toulouse, France
[4]Department of Applied Physics, Universitat Politècnica de Catalunya. BarcelonaTech, Barcelona, Spain
[5]Institute of Space Studies of Catalonia (IEEC-UPC), Barcelona, Spain
[6]National Center for Atmospheric Research, Boulder, Colorado, USA
[7]Uppsala University, Uppsala, Sweden
[8]Institute of Biometeorology - National Research Council (IBIMET-CNR), Florence, Italy

Correspondence to: C. Darbieu
(darc@aero.obs-mip.fr)

Abstract. We investigate the decay of planetary boundary layer (PBL) turbulence in the afternoon, from the time the surface buoyancy flux starts to decrease until sunset. Dense observations of mean and turbulent parameters were acquired during the Boundary Layer Late Afternoon and Sunset Turbulence (BLLAST) field experiment by several meteorological surface stations, sounding balloons, radars, lidars, and two aircraft flying extensively during the afternoon transition. We analyzed a case study based on some of those observations and Large-Eddy Simulation (LES) data focusing on the turbulent vertical structure throughout the afternoon transition.

The decay of turbulence is quantified through the temporal and vertical evolution of (1) the turbulence kinetic energy (TKE), (2) the characteristic length scales of turbulence, (3) the shape of the turbulence spectra. A spectral analysis of LES data, airborne and surface measurements is performed in order to characterize the variation of the turbulent decay with height and study the distribution of turbulence over eddy size.

This study points out the LES ability to reproduce the turbulence evolution throughout the afternoon. LES and observations agree that the afternoon transition can be divided in two phases: (1) a first phase during which the TKE decays with a low rate, with no significant change in turbulence characteristics, (2) a second phase characterized by a larger TKE decay rate and a change in spectral shape, implying an evolution of eddy size distribution and energy cascade from low to high wavenumber.

The changes observed either in TKE decay (during the first phase) or in the vertical wind spectra shape (during the second phase of the afternoon transition) occur first in the upper region of the PBL. The higher within the PBL, the stronger the spectra shape changes.

1 Introduction

The transition from a well-mixed convective boundary layer to a residual layer overlying a stable nocturnal layer raises several issues (Lothon et al., 2014), which remain difficult to address from both modeling and observational perspectives. The well-mixed convective boundary layer with fully developed turbulence is mainly forced by buoyancy. The afternoon decrease of the surface buoyancy flux leads to the decay of the turbulence kinetic energy (TKE), and a change of the structure of the turbulence, which shows more anisotropy and intermittency. It is important to better understand the processes involved, as they can influence the dispersion of tracers in the atmosphere (*e.g.,* Vilà-Guerau de Arellano et al., 2004; Casso-Torralba et al., 2008; Carvalho et al., 2010; Taylor et al., 2014), and the development of the nocturnal and daytime boundary layers of the following days (Blay-Carreras et al., 2014b).

Turbulence decay has been studied with laboratory experiments (*e.g.,* Monin and Yaglom, 1975; Cole and Fernando, 1998), theoretical models (Goulart et al., 2003), numerical studies with Large-Eddy Simulations (LES) (*e.g.,* Nieuwstadt and Brost, 1986; Sorbjan, 1997; Rizza et al., 2013a)and observations (*e.g.,* Fitzjarrald et al., 2004; Grant, 1997; Brazel et al., 2005; Fernando et al., 2004). In all of thoses studies, the decay was mainly related to the decrease of the surface buoyancy flux, but with complexity gained with shear-driven boundary layers (Pino et al., 2006; Goulart et al., 2010), which slow the decay. Using LES, Nieuwstadt and Brost (1986) considered a sudden shut off of surface heat flux, and found that turbulence decay occurred within a period on the order of the convective time scale $t_* = z_i/w_*$, where z_i is the planetary boundary layer (PBL) depth, and w_* is the convective velocity scale (Deardorff, 1970). However, different results were obtained if a slower decrease of the forcing surface buoyancy flux is considered with an external time scale τ_f (Sorbjan, 1997; Rizza et al., 2013a,b; Nadeau et al., 2011). If τ_f is large relative to t_*, the turbulence can adjust to the forcing change, in quasi-equilibrium, as noted by Cole and Fernando (1998). This is the case in the mid-afternoon PBL, when t_* is around 10 or 15 min and τ_f is around 2 or 3 h. Sorbjan (1997) found that the TKE decay scales with τ_f/t_*, with t_* estimated at the start of the decay. But in late afternoon and around sunset, t_* starts to increase significantly (until the definition of w_* is put into question at zero buoyancy flux), and turbulence may not be able to adjust to the external change. Consequently, an extensive description of the turbulence structure is needed to better understand this decay process in the PBL.

The evolution of the turbulence length scales across the afternoon transition has not been addressed extensively, but several studies can be found obtaining diverging results. With fundamental consideration of eddy lifetime, or "turn over" time scale, one may state that smaller eddies will decay earlier than larger eddies (Davidson, 2004). This is one explanation given by Sorbjan (1997), from an LES study, for the increase of the characteristic length scale of the vertical velocity found in the mixed (then residual) layer of the LES. In the surface layer, one may expect the length scales to decrease, as inferred by Kaimal et al. (1972) from the study of surface-layer spectra evolution with stability during the Kansas experiment. With tethered-balloon observations, Grant (1997) indeed showed that the peak of the vertical velocity spectrum shifts to smaller length scales in the surface layer during the evening transition. Finally, Nieuwstadt and Brost (1986) and Pino et al. (2006) found that the length scale of maximum spectral energy of the vertical velocity remained constant during the decay process. By using a theoretical model of the TKE spectrum and LES, Goulart et al. (2010) have also found that the spectral peak remains at approximatively the same wavelength when shear is strong enough to prevent the spectral peak of vertical velocity from shifting towards shorter wavelengths. For other meteorological variables such as the horizontal wind components, temperature and moisture, Pino et al. (2006) have shown that the characteristic length scales increase with time.

The evolution of the turbulence scales remains unclear and only partly understood. It must be thoroughly investigated whether the scales in the mixed and afterward residual layer really increase or not. Considering the time response and equilibrium aspect mentioned above, and the possible decoupling with height between the stabilizing surface layer and the overlying residual layer, it is also important to consider the vertical structure of turbulence decay, i.e. the evolution of turbulence and scales as a function of height. Except Goulart et al. (2010), the numerical studies quoted before (*e.g.,* Sorbjan, 1997; Pino et al., 2006) considered TKE integrated over the entire PBL depth, and observations of the turbulence decay were made most of the time at surface (Nadeau et al., 2011). Only a few observational studies considered the vertical structure of the turbulence afternoon decay (Grant (1997), Fitzjarrald et al. (2004) in the afternoon-decaying PBL).

Here we investigate the evolution of the turbulence spectra and scales from surface to CBL top during the afternoon transition (AT) based on the BLLAST (Boundary Layer Late Afternoon and Sunset Turbulence) dataset, collected during summer 2011 (Lothon et al., 2014). A cloud-free, weak wind day (20 June 2011) is considered for analyzing the evolution of the turbulence, from midday to sunset, by using both observations and an LES model. Our analysis aims at (1) evaluating with a complete observations data set the capabilities of the LES to simulate the turbulence structure of the afternoon decay, (2) analyzing the evolution of integral scales, TKE, shape of the spectra in both observations and numerical simulation, and as a function of height.

The article is organized as follows: In the next section, we present the experimental dataset and describe the case study of the 20 June 2011 through the observations (Section 2). In Section 3, the LES is presented and evaluated with the observations. Our spectral analysis method, used in both observations and LES, is then described in Section 4, before we present and discuss our results (Section 5). Concluding remarks are given in Section 6.

2 Experimental dataset and case study

The BLLAST experiment took place in the south of France, near the Pyrénées mountain range, during the summer 2011. A set of various observational platforms (aircraft, Remotely Piloted Aircraft Systems, balloons) and continuous measurements (towers, remote sensing) monitored the PBL diurnal evolution, focusing on the AT, in various meteorological regimes. BLLAST experiment provides a unique dataset to investigate the vertical structure of the decaying PBL (see Lothon et al. (2014) for a detailed description of BLLAST objectives and experiment).

The experimental dataset used in this study, the chosen study case and its simulation are now described. Note that the site longitude is around 0.21 °E, consequently UTC, very similar to local solar time, is used hereafter as the time reference.

2.1 Experimental dataset

In order to monitor the evolution of the mean structure of the PBL during the AT (and initialize the simulation), we used standard radiosoundings launched every 6 hours, from 0600 UTC to 1800 UTC, and hourly radiosoundings (Legain et al., 2013) of the low troposphere (up to 3 to 4 km), from 1300 to 1800 UTC. The launching sites of the two types of radiosoundings were 4 km apart. The radiosondes measured temperature, water vapour content and the sonde location from which the horizontal wind components were deduced.

Surface energy balance and turbulence structure in the surface layer were provided by several ground stations over different vegetation coverages (wheat, corn, grass, pine forest and moor (composed of heather and gorse)). A permanent 60 m tower provided integrated turbulence measurements in the surface layer above the heterogeneous surface. The statistical moments were estimated over detrended 30 min periods from 10 Hz raw measurements. The surface heat fluxes are used as surface forcing in the simulation.

Two aircraft, the French Piper Aztec (PA) from SAFIRE (Service des Avions Français Instrumentés pour la Recherche en Environnement) (Saïd et al., 2005) and the Italian Sky Arrow (SA) from Ibimet (Istituto di Biometeorologia del CNR) and Isafom (Istituto per i Sistemi Agricoli e Forestali del Mediterraneo) (Gioli et al., 2006), flew extensively during the afternoon, at 65 m s^{-1} and 40 m s^{-1}, respectively. They measured temperature, moisture, pressure, CO_2 mixing ratio and 3-D wind at 50 Hz (SA) and 25 Hz (PA) along 25 to 40 km legs stabilized in attitude and altitude. The detailed instrumentation of both aircraft is given in Lothon et al. (2014).

2.2 Case description

20 June 2011 was selected as our case study on the basis of meteorological criteria and data coverage. The synoptic situation was a high pressure system over the southwest of France, with a light westerly wind leading to fair and cloud-free weather.

Figure 1 shows the normalized altitude z/z_i of the stacked legs flown by the aircraft as well as the different launching times of the radiosoundings (the method used for the PBL height (z_i) estimation is discussed later). The two aircraft flew simultaneously, the PA flying above the SA. They flew along west-east parallel legs, at three latitudes and, as shown in Fig. 1, at six heights within the PBL, and two different time periods: the first one from 1430 UTC to 1530 UTC, the second one later, from 1745 UTC to 1900 UTC. This flight strategy gives access to six heights to study the vertical structure of the turbulence within the PBL.

Figure 2 presents the evolution of the potential temperature (θ) and the wind direction in the PBL at several hours from 0500 to 1800 UTC on 20 June 2011. During the day, the PBL warms by about 7 K and the PBL depth z_i grows up to about 1100 m above ground level. Figure 2a also shows evidence of a warm advection above the PBL between 0515 UTC and 1100 UTC that must be taken into account when simulating. After 1100 UTC, the θ profile hardly changes in the free atmosphere, meaning that the temperature advection is very weak.

Figure 2b shows an easterly wind within the PBL, veering to westerly above. The wind intensity remains constant all along the day (not shown): it is weak within the PBL (less than 4 m s^{-1}) and increases with height, up to 10 m s^{-1} at 1500 m.

The water vapour mixing ratio (r) increases from 8 to 10 g kg^{-1} in the PBL until 1300 UTC and decreases afterward. The temporal evolution of the PBL mean vertical structure is further analysed in section 3.2.

The surface sensible and latent heat fluxes (H and LE, respectively) measured above various vegetation coverages are presented in Fig. 3. The maximum value of H varies from 100-130 W m^{-2} over grass and moor to 450 W m^{-2} over the pine forest. LE shows much less variability between vegetation coverages, maximum values varying from 250 W m^{-2} to 350 W m^{-2}. The measurements at 60 m height integrate a large footprint and should give flux estimates of the heterogeneous landscape. As such, H measured at 60 m height is encompassed in all the others and is close to the moor and grass, the dominant vegetation , which represents about 40% of the vegetation cover over the plateau.

In this study, the AT is defined as the period from the time when the surface buoyancy flux is maximum, to the time where it goes to zero (the surface buoyancy flux is defined as the turbulent vertical transport of vitual potential temperature and is approximated as a linear combination of observed surface sensible and latent heat flux). This period varies according to the surface (Lothon et al., 2014). For the moor coverage, whose surface fluxes will be used to drive the simulation of the 20 June 2011, this period starts at 1200 UTC and ends at 1750 UTC, while it ends 20 minutes earlier when considering H instead of the buoyancy flux. This delay is observed for all the intense observation period (IOP) days of the BLLAST campaign implying that the latent heat flux reaches its minimum value systematically later than the sensible heat flux. Thus, the forcing time scale of the surface flux decay τ_f is around 5.8 hours over the moor surface.

3 LES

As a complementary tool, a LES is initialized with the BLLAST observations to study turbulence decay of convec-

tive boundary layer over an homogeneous and flat surface. The observations from the 20 June are used to guide our simulation, like the 1 July and 25 June guided the studies of Blay-Carreras et al. (2014b) and Pietersen et al. (2015) respectively. Our aim is not to reproduce a real case but rather to use the BLLAST dataset as a benchmark to simulate a boundary layer with the same range of thermal and dynamical instabilities than those observed during BLLAST.

3.1 LES configuration and initilization

Our LES is initialized with early morning radiosoundings and forced with homogeneous surface fluxes, based on those measured over the moor surface. Temperature and humidity advection are prescribed. The lateral boundary conditions are periodic.

The LES code from National Center for Atmospheric Research (Moeng (1984), Sullivan and Patton (2011), Patton et al. (2005), Lohou and Patton (2014)) is based on the Boussinesq equations, including conservation laws for momentum, mass and the first law of thermodynamics. The subgrid-scale model includes a turbulent-kinetic-energy eddy-viscosity model suggested by Deardorff (1980), used by Moeng (1984) and improved by Sullivan et al. (1994).

The simulation resolves a domain of 10.24×10.24 km^2 horizontally and 3.072 km vertically, with Δx $= \Delta$y $= 40$ m and Δz $= 12$ m of horizontal and vertical resolution, respectively. This results from a compromise between the computation time and three constraints: (1) the domain size and resolution were chosen after a sensitivity study (not shown) so that the LES spectra were able to represent the main characteristics of the observed spectra, (2) the resolution was chosen so that the ratio of z_i to $(\Delta x \times \Delta y \times \Delta z)^{1/3}$ was large enough to ensure that the results are independent of the resolution (Sullivan and Patton, 2011), and, (3) the ratio of Δx to Δz was kept rather small, but with a high enough vertical resolution to correctly represent the entrainment zone (Sullivan and Patton, 2011). The time step evolves during the simulation and is about 1.4 s for fully convective conditions.

The simulation was initialized early in the morning, in order to ensure a fully turbulent convective PBL by the afternoon. The wind, potential temperature and specific humidity initial profiles for the LES were deduced from the 0515 UTC radiosounding (see dashed lines in Fig. 2 for temperature and wind speed). No geostrophic wind is prescribed. This simple representation of the wind leads to a simulation with very low wind speed as it is the case in the observations, but does not allow to simulate the shear in wind direction. An homogenous and flat surface is considered in the LES with imposed surface fluxes which are those measured at the moor site (Fig. 3).

Vertical profiles of large-scale total advection (horizontal plus vertical advection) of heat and moisture were hourly prescribed in the simulation and linearly interpolated in between. They were derived from AROME (Seity et al., 2011) forecast model (horizontal resolution of 2.5 km), using the 16 grid points in a box surrounding the experimental site. This model confirms predominant zonal advection, especially during the morning.

From 0515 UTC to 1000 UTC, the temperature advection is important and about 10 K day^{-1} from 500 m up to 1500 m (not shown). After 1100 UTC, it decreases and is negligible in the afternoon. This is consistent with what is observed on the evolution of the potential temperature (Fig. 2a). From sunrise to 1400 UTC, the moisture advection is about -10 g kg^{-1} day^{-1} from the surface up to 500 m, and about 10 g kg^{-1} day^{-1} above. After 1400 UTC, the moisture advection weakens (not shown).

The data files used to run this case (initial profiles, surface flux and advection profiles) are available on the website of the BLLAST database (http://bllast.sedoo.fr/database).

3.2 Evaluation of the simulated boundary layer

The bracket notation $\langle\psi\rangle$ for any simulated variable ψ is used to represent the 2D-horizontal average over the LES domain. The same notation is used for the 1D-horizontal average of the airborne measurements along the legs. For the surface dataset, $\bar{\psi}$ represents the time average notation. For these three types of datasets, the turbulent fluctuations ψ' are defined as deviations from the corresponding mean. For a more fair comparison with the simulated variances, the observed variances are estimated by integration of the spectra over the wavenumber range resolved in the simulation. At last, all the simulated mean vertical profiles are averaged over 30 min and noted for simplicity with the bracket notation $\langle\psi\rangle$, which then indicates both horizontal and temporal average.

The evolution of the simulated θ vertical profiles is compared with observations in Fig. 4a from 0530 to 1750 UTC. The simulated θ is close to the observations in the mixed layer (differences lower than 0.1 K) and in the free atmosphere, simulating the change in θ profile between 0515 UTC and 1115 UTC due to the prescribed advection.

In the first 100 m, the differences of stability profile at 1130 UTC might be due to the different locations of the soundings and the moor site where the surface flux is observed. The 1730 UTC LES profile is already neutral, whereas the observations at 1750 UTC still has a superadiabatic region. The differences are due to the fact that as soon as the surface buoyancy fluxes turn negative, the LES potential temperature profile becomes stable at the lower layers of the BL. This delay between the time when the buoyancy flux goes to zero and the time when the local gradient of virtual potential temperature changes sign has been observed and analyzed in (Blay-Carreras et al., 2014a). It can be of the order of 30 min to 1 hour.

Figure 4b presents the evolution of the water vapour mixing ratio. The temporal evolution of r profiles shows a well simulated daily humidification. One can notice a 1 g kg^{-1} departure at 1305 and 1750 UTC than actually observed.

The horizontal mean wind speed is well reproduced in the simulation during the day: the wind remains weak and about 2 m s^{-1} in the PBL. u_* evolves from 0.2 to 0.1 during the afternoon for both observed and simulated data. The wind increases with altitude above the PBL and reaches 10 m s^{-1} at 2000 m. No wind forcing is prescribed in the simulation, therefore the observed wind direction change from West to East within the mixed layer between 0530 and 1130 UTC is not simulated (Fig. 4d). Whilst the wind speed shear is well simulated, the wind direction shear is evidently underestimated. Consequently, shear-driven processes (Pino et al., 2006) might not be as important in the simulation as in the observations.

The simulated vertical profiles of the buoyancy flux normalized by the surface buoyancy flux at the start of the AT (Fig. 5) have a quite classical shape until 1330 UTC with a linear decrease with height and negative flux above 0.8 z_i. In the simulation, z_i is estimated as the height of the mixed layer, determined with a threshold on the θ vertical gradient (0.01 K m^{-1}). This method was prefered to the one used for radiosoundings (see below) because of the complex humidity profiles which lead to more fluctuating z_i estimates. However, the difference between these two estimates is less than 50 m. After 1330 UTC, the upper layer characterized by negative entrainment flux deepens and goes down to 0.6 z_i at 1800 UTC. During the AT the entrainment rate (ratio of the buoyancy flux at the top of the PBL to the buoyancy flux at surface) remains constant and about - 0.13 (not shown). Unfortunately, this value cannot be compared to observations since the fluxes deduced from airborne measurements in the PBL vary substantially at that time, and because of lack of statistics of the large scales in a less and less stationary PBL. Long enough aircraft legs to get accurate statistical moment estimates in convective PBL (Lenschow et al., 1994) are even more relevant during the AT.

The temporal evolution of z_i has been estimated from Ultra High Frequency radar wind profiler (hereafter UHF) and radiosounding measurements and compared to the simulation (Fig. 6). z_i is estimated from UHF as the maximum of the refractive index structure coefficient (Heo et al., 2003; Jacoby-Koaly et al., 2002). From radiosoundings, z_i is estimated as the altitude of the maximum relative humidity below 2500 m (this criterion has been shown to be consistent in time and height during BLLAST experiment (Lothon et al., 2014)).

Until 0900 UTC, the UHF detects the residual layer of the previous day. After 1000 UTC, the z_i increase is similarly depicted by the UHF and radiosoundings, with a maximum value of 1100 m. The simulated PBL grows slower than the observed PBL and reaches 850 m. This discrepancy between observed and simulated z_i (which is larger than the uncertainty of z_i estimate) might be partly explained by a weaker entrainment effect in the simulation due to a lack of wind shear.

The temporal evolution of the simulated and observed TKE at several heights is presented in Fig. 7. The TKE reads

$$TKE(z,t) = \frac{1}{2}(\sigma_u^2(z,t) + \sigma_v^2(z,t) + \sigma_w^2(z,t)), \quad (1)$$

where σ_u^2, σ_v^2 and σ_w^2 are the variances of the horizontal u, v, and vertical w wind components. For a better comparison, simulated and observed TKE are estimated using the wind components variances deduced from the integration of the spectra over the wavenumber range of the simulation. By doing this, the TKE associated with large and small eddies observed, but not simulated or resolved in the LES, is removed from the observed TKE. Even with this method, LES underestimates the observed TKE by a factor sometimes as high as 1.5.

In summary, the simulated boundary layer is comparable to the observed one in terms of boundary layer height, wind speed, and dynamical and thermal stability (not shown) near the surface. The lower development of the PBL height of about 200 m and the underestimated TKE by a factor of 1.5 can be partly explained by the directional wind shear which is not simulated. The latter might increase the entrainment and the turbulence dynamical production at the top of the boundary layer. Despite these differences on the main PBL structure, the simulation is realistic enough to evaluate how the turbulence evolves in a convective boundary layer during the AT and the comparison of simulated and observed boundary layer will be analyzed accordingly.

4 Spectral analysis method

A broad overview of the turbulent conditions during the afternoon is depicted through the analysis of the TKE temporal evolution at different heights in the PBL.

The energy distribution among the different eddy scales is then studied through a spectral analysis of the vertical velocity w within the entire PBL. The evolution of w spectral characteristics is analyzed by use of an analytical spectral model.

This study focuses on w because simulated and observed w spectra are more easily comparable than the spectra of the horizontal components. Indeed, the horizontal components have significant energy at low wavenumber (large scales) in the observations which can not be represented in our simulated domain.

The choice of the analytical spectra is now discussed since several models exist for convective conditions. Among others, the Kaimal et al. (1972) and Kaimal et al. (1976) formulations were established from Kansas experiment observations for the surface layer and from Minnesota experiment observations for the mixed layer. The von Kàrmàn spectral model (Kàrmàn, 1948) is also widely used for isotropic turbulence. Højstrup (1982) proposed a more generalized model for w spectra up to $z/z_i = 0.5$, based on a stability function from neutral to very unstable conditions. However, many

of these analytical models were validated for unstable near surface conditions and most of them are not suitable within the entire convective PBL (Lothon et al., 2009). Among several analytical models tested, the general kinematic spectral model for non-isotropic horizontally homogeneous turbulent field from Kristensen and Lenschow (1989) (named hereafter $KL89$) is the one which best fits the observed spectra at surface and in the boundary layer acquired during the BLLAST field campaign (not shown). For w, the $KL89$ model writes:

$$\frac{S_{Kris}(k)}{\sigma_w^2} = co\frac{l_w}{2\pi}\frac{1+\frac{8}{3}(\frac{l_w k}{a(\mu)})^{2\mu}}{(1+(\frac{l_w k}{a(\mu)})^{2\mu})^{5/(6\mu)+1}}, \quad (2)$$

where

$$a(\mu) = \pi\frac{\mu\Gamma(\frac{5}{6\mu})}{\Gamma(\frac{1}{2\mu})\Gamma(\frac{1}{3\mu})}, \quad (3)$$

k being the wavenumber along the trajectory of the airplane, or along the west-east axis in the simulation (which is also the mean wind direction in the simulation), and in the mean wind direction for surface measurements. Γ is the gamma function. co is a coefficient which adjusts the amount of energy because σ_w^2 is calculated over a limited range of wavenumbers. This model has two other characteristic parameters: the integral length scale l_w, which is a characteristic scale corresponding to the scales over which w remains correlated with itself (Lenschow and Stankov, 1986), and a sharpness parameter μ, which governs the curvature of the spectra in the region of the peak, between the low wavenumber range and the inertial subrange. The larger μ, the sharper the peak. According to Eq. 2, the $KL89$ model gives the Kaimal et al. (1972) spectrum for μ =0.5 and the Kàrmàn (1948) spectrum for μ =1. It is thus a more generalized model, able to adapt to a larger range of conditions. Note that l_w is related to the wavelength of the energy density maximum (Λ_w) by a monotonic function of μ:

$$\Lambda_w = \left\{\frac{5}{3}\sqrt{\mu^2+\frac{6}{5}\mu+1}-(\frac{5}{3}\mu+1)\right\}^{\frac{1}{2\mu}}\frac{2\pi}{a(\mu)}l_w. \quad (4)$$

This model is fit to each observed and LES spectrum, by finding the best [co, l_w, μ] triplet using a logarithmic least squares difference method.

The integral scale of w is usually defined from w autocorrelation function R_w as:

$$L_w = \int_0^\infty R_w(r)dr, \quad (5)$$

where r is the displacement in space or time. L_w gives an estimate of the horizontal size of the convective thermals in the boundary layer. In this study, L_w is obtained using an integration until the first zero of $R_w(r)$ (Lenschow and Stankov, 1986). It is used here as a reference to which l_w is compared.

In this $KL89$ analytical spectrum, anisotropy of turbulence is taken into account by varying integral scale from transverse to lateral spectra. Even considering anisotropy, the spectrum follows the usual -5/3 slope in the inertial subrange.

For surface-based spectra, 30-min samples are used, which is a good compromise between a sufficient number of eddies and stationary conditions. The spectra based on the aircraft measurements are calculated on 35 km long legs on average. To ensure consistency between simulated and observed spectra, one-dimensional simulated spectra are considered in the LES. They are calculated along the west-east direction and averaged along the north-south direction. Simulated spectra are estimated above the fourth vertical level (to ensure a negligible contribution of the subgrid scale) and every 96 m in the vertical. The same sampling is used to calculate the autocorrelation functions for L_w estimates.

In order to study the evolution of the spectral slopes in specific domains, the wavenumber range is split into three parts: (1) the low wavenumber range $[0, k_1]$, (2) the region, $[k_1, k_2]$, around the maximum energy density at $k = 2\pi/\Lambda_w$, (3) the inertial subrange $[k_2, \infty[$. The limits are defined here as $k_1 = \pi/\Lambda_w$ and $k_2 = 4\pi/\Lambda_w$.

An important part of the study is to verify the level of agreement between the observed or LES spectra and the $KL89$ analytical model fit. A quality index of the analytical fit is, therefore, estimated based on the ratio between the observed (respectively LES) spectrum and the analytical spectrum:

$$IQ_{OBS} = \frac{1}{N_{OBS}}\sum_k\left|\log\left(\frac{S_{OBS}(k)}{S_{KL89}(k)}\right)\right|, \quad (6)$$

$$IQ_{LES} = \frac{1}{N_{LES}}\sum_k\left|\log\left(\frac{S_{LES}(k)}{S_{KL89}(k)}\right)\right|, \quad (7)$$

where S_{OBS} is the spectrum calculated from the observed w, S_{LES} is the spectrum calculated from the simulated w, and S_{KL89} is the analytical spectrum given by Eq. 2 that best fits the observed or simulated spectra. N is the number of k values on which S is defined. The larger IQ_{OBS} (IQ_{LES}), the larger the departure between the observed (simulated) and the analytical spectra. No threshold can be found for these fit quality criteria, therefore values of IQ_{OBS} and IQ_{LES} in convective conditions (from 1200 to 1400 UTC) are used as reference.

Figure 8 presents the normalized spectra of w from both aircraft and simulated data, fitted with the $KL89$ analytical spectra model. The aircraft (simulated) spectra are calculated at 1500 UTC and 1800 UTC and at $z = 0.6z_i$ ($z = 0.6-0.75z_i$ slice-averaged). This figure shows first, the ability of the simulation to properly reproduce both the energy production domain and the inertial subrange, and second,

the ability of the analytical spectral model to fit well the observed and simulated spectra in mid-afternoon convective conditions (1500 UTC) and at the end of the afternoon (1800 UTC).

For those two examples, $IQ_{OBS} = 0.11$ and $IQ_{LES} = 0.02$ at 1500 UTC, and $IQ_{OBS} = 0.10$ and $IQ_{LES} = 0.015$ at 1800 UTC. In general, the quality index for the observations are about 5 to 10 times larger than for the LES (not shown). This is due to the lack of statistics at large scales in observations, leading to larger fluctations in the spectral density energy for the first domain (low wavenumbers), whereas the LES spectra are averaged along the north-south direction, reducing the variability.

We also found that the quality index for observed and simulated data generally remained constant until 1900 UTC, except a slight increase of IQ_{LES} for data above 0.6 z/zi after 1830 UTC. This means that the spectra fit is equally reliable throughout the AT, allowing the study of the time evolution of the spectra characteristics from the convective conditions until near neutral conditions. This result should be highlighted in the case of simulated spectra given the overly dissipative nature of the subgrid-scale models in the LES (Meneveau and Katz, 2000).

The spectra changes throughout the AT are already noticeable in Fig. 8: Λ_w shifts toward smaller wavelength, l_w increases, the spectra flatten and the inertial subrange slope changes. This is further quantified and discussed in the following section.

5 Results

5.1 TKE decay within the entire PBL

Most previous studies investigated either vertically integrated simulated TKE over PBL depth, or measured TKE in the surface layer. The TKE decay according to height remains sparsely documented (Grant, 1997; Goulart et al., 2010).

Figure 9a shows the evolution of half-hour averaged hourly vertical profile of simulated TKE from 1130 UTC to 1830 UTC. The profiles show that TKE decreases within the whole depth of the PBL, but that there is a one-hour delay between the start of the decay at the top and the start at the bottom: at 1230 UTC, the TKE continues to increase in the lower PBL, while it has started to decrease in the upper part. After 1530 UTC, the decay is homogeneous over the vertical. This differential TKE decay will be named TKE top-down decay hereafter. This result is consistent with Grimsdell and Angevine (2002) and Lothon et al. (2014) studies which revealed, with remote sensing observations, a decay of TKE dissipation rates from top to bottom. Shaw and Barnard (2002) also studied the decay with Direct Numerical Simulation (DNS), based on a realistic surface flux decay. They found that the turbulence is maintained at the surface relative to upper layers, which they explain with shear at the surface.

In this study, the simulation shows this top-down evolution likely because the shear in wind direction at the top of the boundary layer is weak and does not maintain the dynamical turbulence production. We can expect a reduced top-down effect in the reality since there is shear in direction which is not simulated.

Turbulence anisotropy (see Fig. 9b), considered here as the ratio of the horizontal to the vertical wind variances, gives highlights on the turbulence structure evolution during the TKE decay. Before 1630 UTC, turbulence anisotropy remains smaller than unity in the mid-PBL, which is in agreement with the dominant vertical motion of the convective eddies. In the upper and lower parts of the PBL, turbulence anisotropy is larger than unity, due to small vertical velocity variance close to the surface and the entrainment zone (so called 'squashed' turbulence (Lothon et al., 2006)).

The anisotropy ratio becomes larger than one only after 1730 UTC in the middle of the PBL, but increases close to the top as early as 1230 UTC. The change in anisotropy, like the TKE, starts early in the upper PBL, with an increasing momentum transfer from vertical to horizontal components during the decay process.

5.2 Spectral analysis

5.2.1 Evolution of the vertical velocity's spectral slopes

The slopes of the simulated and observed spectra are first analyzed because (1) they are key characteristics of the turbulence spectra and, (2) the $KL89$ spectral model assumes for $kS(k)$ the theoretical slope of 1 and $-2/3$ for low and high wavenumber range, respectively. The slopes are estimated by linear regression on $kS(k)$ for the wavenumber first and third ranges defined in Section 4.

In the low wavenumber range, the slopes of the simulated and near-surface observed spectra are close to the theoretical value of 1 and remain approximately constant during the whole day (see Fig. 10a). The spectral slopes of airborne measurements are steeper than the theory predicts and vary from 1.5 to 2.5. This result illustrates the weak statistical representativity of large scales along aircraft flight leading to scattered spectra slope estimates in this wavenumber range.

In the inertial subrange, both simulated and aircraft data reveal steeper slopes than the theoretical value of - 2/3, even during the fully convective period (Fig. 10b). Steeper inertial subrange slopes were previously observed with vertically pointing ground based lidar (Lothon et al., 2009) and with airborne high frequency in situ measurements (Lothon et al., 2007)). The theoretical -2/3 slope is based on the hypothesis of isotropic turbulence. Therefore, a possible explanation for these steeper slopes in convective conditions could be the loss of isotropy in real conditions and in particular the role of convective structures and the associated anisotropy.

As mentioned before, in section 5.1, they are responsible for anisotropy smaller than one. We believe that the more 'coherent' or organized the w field, the smaller the anisotropy and the steeper the slope. But this explanation needs further work for confirmation. At the end of the afternoon, the slopes consistently flatten in both LES and aircraft data. This flattening appears to behave differently according to height in two ways: (1) it occurs earlier at the top of the PBL (around 1600 UTC) than in the lower layers (after 1745 UTC at $0.15z_i$), (2) the lower in the PBL, the smaller the flattening. These delayed and reduced changes with decreasing altitude are consistent with the constant - 2/3 slope during the whole day near the surface.

5.2.2 Characteristic length scales

The integral scale is one of the two spectral characteristics determined from the fit of the $KL89$ analytical spectral model.

We verified that these integral scale estimates (l_w) were similar to estimates of integral scales (L_w) based on the autocorrelation function (Eq. 5) which is more generally used. The two methods were found to be consistent with each other and to give similar temporal evolution of integral scale (not shown). Hereafter, only l_w is considered.

The temporal evolution of l_w obtained with aircraft and surface data and with the simulation at different heights, is presented in Fig. 11. At midday, the length scales verify what is found in literature, with a value around 200 m (about $0.2z_i$) in the middle of the mixed layer (Lenschow and Stankov (1986) with aircraft observations and Dosio et al. (2005) with LES, among others). Smaller length scales are observed and simulated at the top and at the bottom of the mixed layer because of 'squashed' eddies near the interfaces. l_w remains approximately constant until 1700 UTC, and then increases above $0.15z_i$ for both LES and aircraft data. The higher the considered level, the sharper the l_w increase.

Close to surface, l_w remains constant until 1700 UTC at a value of 10 m, then decreases to 5 m. As expected, the 60 m mast data provide longer l_w than at the surface, but with a large scatter (between 30 and 80 m) making difficult the estimate of l_w tendency with time at that height.

5.2.3 Shape of the spectra

The spectral shape is depicted by the μ sharpness parameter (Eq. 2). Figure 12 shows the temporal evolution of μ that gives the best fit of the spectra for simulation, aircraft and surface data. Above 0.15 z_i, μ remains constant at a value of about 2 until 1600 UTC, aircraft and simulated data giving similar results. Those results are similar to those found by Lothon et al. (2009) with ground-based lidar, who also observed sharper spectra than Kaimal spectra ($\mu = 0.5$) in the middle of the PBL. After 1600 UTC, μ decreases, meaning that the turbulence spectra flatten during the late afternoon transition associated with a broadening of the energy containing wavenumber range above 0.15 z_i. This seems consistent with the theoretical spectral analysis by Goulart et al. (2010) (see their Fig. 6 bottom in the convective boundary layer). On the contrary, close to surface and at 60 m height, $\mu \approx 0.5$ throughout the day, which corresponds to the spectral model from Kaimal et al. (1972) and means that the energy wavenumber range remains large during the LAT. In $KL89$ analytical model, μ, l_w and Λ_w are linked by Eq. 4 which gives higher Λ_w/l_w for higher μ (Lenschow and Stankov, 1986). As noticed in Fig. 8, Λ_w drifts slightly toward smaller eddies. Keeping in mind that Λ_w represents the distance between two structures and l_w represents the width of a structure, this means that during the LAT, the thermals become closer to each others whereas the increase of l_w means the thermals become larger. This is consistent with a decreasing skewness of w as time evolves, which we do find in both observation and LES (not shown).

5.3 Timing of the changes

The previous results illustrate the changes of turbulence characteristics throughout the afternoon according to height. The times when these characteristics start to change are now quantified using the simulation data above $0.15z_i$, the tower measurements at 60 m and the near surface moor and corn data. The time of change for a parameter x is noted t_x (Fig. 13). For μ, l_w and the slope, it is the time when the decay rates of these spectra parameters depart from their mean value by more than three times their standard deviation (the decay rates are estimated over 1.5 h and their means and standard deviations are calculated between noon and 1400 UTC). Because of the diurnal cycle of the TKE and the horizontal and vertical velocity variances, this method could not be applied to determine the time change of these parameters. t_{TKE}, $t_{<w'^2>}$ and $t_{<u'^2>+<v'^2>}$ were thus the time when the decaying rate of the parameter (estimated by linear regression over 1.5 h) becomes larger than an arbitrary threshold of -0.02 m^2 s^{-3}.

As already noticed in section 5.1, the TKE first decreases at the top of the boundary layer half an hour after the start of the AT (Fig. 13). That is, once the surface flux starts to decrease, the surface-driven turbulence does not rise up to the top of the CBL anymore. This indicates that turbulence decreases first at the top of the PBL, whereas it is maintained longer under 0.15 z_i. The TKE decrease is exclusively driven by the vertical velocity variance, which decreases at the top of the PBL one and half hour before the maximum of the surface buoyancy flux. The early decrease of the vertical velocity variance is counter-balanced in TKE by the delayed change of the horizontal wind variance. This implies an increase in the anisotropy of the velocity variances in the early stage of surface flux decrease.

The change in other spectral parameters (length scale, sharpness and slope) is observed much later, during the last

two hours before the zero surface buoyancy flux. The vertical profiles of t_{l_w}, t_{slope} and t_μ, indicate an increase of integral scales, a flattening of the inertial subrange slope and a flattening of the spectra, appearing first at the top of the boundary layer and rapidly reaching the lower layers.

Near the surface and at 60 m, a very weak evolution of the spectra is observed. The spectra keep the same sharpness, similar to Kaimal spectra, with a constant slope of - 2/3 in the inertial subrange, and a very slightly decreasing l_w. These results are in continuity with the spectra behavior above 0.15 z_i. Indeed, μ decreases from around 2 in convective conditions to 0.5 at the end of the AT in the whole upper layer and the l_w increase in the upper layers is less and less pronounced with decreasing height.

5.4 Discussion

The above analysis of the evolution of the turbulence structure during the AT suggests us to separate this period in two stages: early and late afternoon.

In the early afternoon, from the occurrence of the buoyancy maximum until about two hours before sunset, (1) the TKE decreases within the whole PBL, with a one-hour delay between the upper part (earlier decay) and the lower part of the PBL (postponed decay), (2) the vertical profile of anisotropy does not change much within the PBL, except close to the top, and (3) the spectra maintain the characteristics of the fully-developed convective boundary layer, with similar integral scales and sharpness parameter.

In the late afternoon, from two hours before sunset until when the surface buoyancy flux reduces to zero, (1) the TKE decreases more rapidly than during the early AT within the whole PBL, (2) turbulence anisotropy increases abruptly within the PBL, starting initially near the PBL top, and (3) the shape of the spectra evolves, with a decrease of the sharpness parameter, a flattening of the inertial subrange slope, an increase of the integral length scales in the mid and upper PBL. The higher in the PBL, the stronger the increase of the integral scales, with very slight changes of the spectra shape observed close to the surface.

The two stages of the TKE decay found in this study remain consistent with previous results found by Nadeau et al. (2011) and Rizza et al. (2013a). Both authors showed a decrease of the TKE following a t^{-n} power law with a continuous increase of n. Nadeau et al. (2011) defined two main stages characterized by n around 2 and 6 respectively. Rizza et al. (2013a) added a preliminary stage with n equal to 1. Our first stage includes t^{-1} and t^{-2} power laws, and the second one includes t^{-6}. However, it seems somehow arbitrary to characterize our two stages by a specific value of n since it evolves continuously. This study focuses on the link between the structure of the turbulence and the TKE evolution. Also, the TKE budget evolution in time was of any help to explain the two stages of the TKE decrease. Whilst the different terms do decrease with time, their respective contribution to the TKE tendency hardly changes from the first to the second stages (not shown).

Our understanding of the two different stages of the AT is that during the early afternoon, the buoyancy flux remains large and its decay is slow enough, to give time to the PBL to adjust to the change and to remain in quasi-steady balance. In other words, the convective time scale t_* is small enough ($\sim$ 9 min) relative to τ_f ($\sim$ 5.8 h), to allow this quasi-steady state. The spectral characteristics remain similar to what they are at maximum surface buoyancy flux. Buoyancy remains a dominant influence during this stage, which leaves predominance to the vertical velocity variance and convective structures. The latter, with a characteristic horizontal length typically linked to the PBL depth, could maintain a sharp spectral peak. Predominance of convective structures might also be at the origin of the steep inertial subrange slope. Close to surface, where these convective structures are not yet well shaped, inertial subrange slope is - 2/3.

On the contrary, during the late afternoon, t_* increases (about 20 min at 1700 UTC) and the buoyancy flux gets too small for the PBL to maintain the vertical consistency of the turbulence structure from surface up to the top of the PBL. The impact of surface buoyancy decreases faster than that of entrainment during this period: although the entrainment flux magnitude diminishes, entrainment occurs over a broader vertical depth extending down to $0.6z_i$ (Fig. 5).

An increase of the entrainment role could explain the increase of the vertical velocity integral scales (Lohou et al. (2010) and Canut et al. (2010)), which is observed in the upper PBL during the late afternoon during our BLLAST case. The increase in vertical velocity integral scales is consistent with the results of Sorbjan (1997) but differs from those of Pino et al. (2006). This could be due to the progressive cease of the surface flux in Sorbjan (1997) and Grant (1997), versus the sudden shut-off in Pino et al. (2006). In the surface layer, the decrease of the integral scales is consistent with the observations made by Grant (1997) and with the results of Kaimal et al. (1972).

The flattening observed in the inertial subrange during the late afternoon is difficult to explain because one could expect a steeper slope in inertial subrange when the flow becomes less turbulent, assuming that the smaller scales will dissipate faster than the larger scales. However, hypotheses could be made to explain the observed flattening of the spectra in the inertial subrange: (1) the increase of anisotropy might be associated with such a change of the cascade, (2) if the turbulence is now freely decaying, without influence of coherent structures and vertical velocity dominance, the cascade could become more efficient, resulting in flattening slope according to Moeng and Wyngaard (1988). In any case, it seems that with the turbulence being no longer fully forced, the criteria for locally isotropic turbulence are no longer met. The theoretical model of TKE spectrum proposed by Goulart et al. (2010) could be an interesting tool to further understand this slope change since it considers anisotropy of turbulence

through the $KL89$ analytical spectrum, but also into some of the terms of the TKE budget which might impact on the inertial subrange slope.

The progressive shut-off of the surface heat fluxes is shown to be an important aspect of the AT. Nieuwstadt and Brost (1986) and Pino et al. (2006) who analyzed simulations with a sudden shut-off of the buoyancy flux pointed out what they called a demixing process, which infers a negative buoyancy flux within the whole PBL. The impact of entrainment in that case might be overestimated. Similar to Sorbjan (1997), when progressively transitioning through the afternoon from surface buoyancy dominated to entrainment dominated regime, the demixing process is strongly reduced and limited to the half-upper part of the PBL.

One might wonder whether these results could be impacted by the initial conditions. The use of all the airborne measurements acquired during the BLLAST experiment shows the general trend of an increasing integral scale during the late afternoon (not shown). However, it would be useful to complete this study with some additional simulations either targeting other BLLAST IOPs or performing some sensitivity analyses. Wind shear could be an important focus as Nieuwstadt and Brost (1986), Pino et al. (2006) or Goulart et al. (2010) found that strong wind shear at the top and bottom of the PBL delays the decay.

6 Conclusions

This study is based on the use of analytical spectra to depict and quantify changes in the vertical velocity spectra throughout the AT and according to height. BLLAST aircraft and surface station measurements are used to study the turbulence spectral evolution on 20 June 2011. A Large-Eddy Simulation constrained by observed conditions during BLLAST, but significantly simplified, allows us to investigate a continuous spectra analysis in time and height.

The simulated data, even with simplified forcings and initial conditions, are in a satisfactory agreement with the airborne, radiosonde and surface observations. The model reasonably simulates the turbulence structure through the afternoon with a resolution and a domain size allowing a good fit of the simulated spectra with the Kristensen and Lenschow (1989) analytical model above $0.15z_i$.

Two main conclusions can be drawn from this study, giving essential highlights on the turbulence evolution in time and height:

(1) This study shows for the first time the different steps occurring during the AT, which is defined as the period starting at the maximum surface buoyancy flux and ending when the buoyancy flux reaches zero. The early afternoon (first phase from 0 to $0.75\tau_f$) is characterized by a low-rate decrease of the energy level, but the turbulence characteristics remain similar to those during fully convective conditions: similar turbulence length scales and cascade characteristics from large to small eddies. During the late afternoon (second phase from 0.75 to $1\tau_f$), TKE decay rates increase and turbulence characteristics evolve rapidly implying very different eddy size and energy transfer.

(2) The second important point concerns the turbulence evolution along the vertical. The changes observed either in TKE decay (during the early afternoon) or in w spectral shape (during the late afternoon) start at the top of the boundary layer. Furthermore, the higher within the PBL the stronger the spectra shape changes. These results show that the top of the boundary layer is first affected by the changes.

Acknowledgements. The BLLAST field experiment was made possible thanks to the contribution of several institutions and supports : INSU-CNRS (Institut National des Sciences de l'Univers, Centre national de la Recherche Scientifique, LEFE-IMAGO program), Météo-France, Observatoire Midi-Pyrénées (University of Toulouse), EUFAR (EUropean Facility for Airborne Research) BLLATE-1&2, COST ES0802 (European Cooperation in the field of Scientific and Technical) and the Spanish MINECO projects CGL2009–08609, CGL2012–37416–C04–03, and CGL2011-13477-E. The field experiment would not have occurred without the contribution of all participating European and American research groups, which all have contributed in a significant amount. The Piper Aztec research airplane is operated by SAFIRE, which is a unit supported by INSU-CNRS, Météo-France and the French Spatial Agency (CNES). BLLAST field experiment was hosted by the instrumented site of Centre de Recherches Atmosphériques, Lannemezan, France (Observatoire Midi-Pyrénées, Laboratoire d'Aérologie). Its 60 m tower is partly supported by the POCTEFA/FLUXPYR European program. BLLAST data are managed by SEDOO, from Observatoire Midi-Pyrénées. Since 2013, the French ANR supports BLLAST analysis. See http://bllast.sedoo.fr for all contributions. We particularly thank Eric Pardyjak, Oscar Hartogensis, Dominique Legain, and Frédérique Saïd, for providing the surface measurements used in this study. We are also grateful to Bruno Piguet for the first processing of the Piper Aztec dataset and to Dominique Legain and the CNRM-4M team for the frequent radiosoundings. Computer facilities for the Large Eddy Simulation were provided by CALMIP (Calcul en Midi-Pyrénées, France).

References

Blay-Carreras, E., Pardyjak, E., Pino, D., Alexander, D., Lohou, F., and Lothon, M.: Countergradient heat flux observations during the evening transition period, Atmospheric Chemistry and Physics Discussion, 14, 7711–7737, 2014a.

Blay-Carreras, E., Pino, D., Van de Boer, A., De Coster, O., Darbieu, C., Hartogensis, O., Lohou, F., Lothon, M., Pietersen, H., and Vilà-Guerau de Arellano, J.: Role of the residual layer and large–scale subsidence on the development and evolution of the convective boundary layer, Atmospheric Chemistry and Physics, 14, 4515–4530, 2014b.

Brazel, A., Fernando, H., Hunt, J., Selover, N., Hedquist, B., and Pardyjak, E.: Evening Transition Observations in Phoenix, Arizona, Journal of Applied Meteorology, 44, 99–112, 2005.

Canut, G., Lothon, M., Saïd, F., and Lohou, F.: Observation of entrainment at the interface between monsoon flow and the Saharan Air Layer, Quarterly Journal of the Royal Meteorological Society, 136, 34–46, 2010.

Carvalho, J., Degrazia, G., Anfossi, D., Goulart, A., Cuchiara, G. C., and Mortarini, L.: Simulating the characteristic patterns of the dispersion during sunset PBL, Atmospheric Research, 98, 274–284, 10.1016/j.atmosres.2010.06.009, 2010.

Casso-Torralba, P., Vilà-Guerau de Arellano, J., Bosveld, F., Soler, M., Vermeulen, A., Werner, C., and Moors, E.: Diurnal and vertical variability of the sensible heat and carbon dioxide budgets in the atmospheric surface layer, Journal of Geophysical Research, 113, D12 119, 10.1029/2007JD009583, 2008.

Cole, G. and Fernando, H.: Some aspects of the decay of convective turbulence, Fluid Dynamics Research, 23, 161–176, 1998.

Davidson, P.: Turbulence: An introduction for Scientists and Engineers, Oxford University Press Inc., New York, 2004.

Deardorff, J.: Convective velocity and temperature scales for the unstable planetary boundary layer and for Rayleigh convection, Journal of the Atmospheric Sciences, 27, 1211–1215, 1970.

Deardorff, W.: Stratocumulus-capped mixed layers derived from a three-dimensional model, Boundary Layer Meteorology, 18, 495–527, 1980.

Dosio, A., Vilà-Guerau De Arellano, J., and Holtslag, A. A. M.: Relating Eulerian and Lagrangian Statistics for the Turbulent Dispersion in the Atmospheric Convective Boundary Layer, Journal of the Atmospheric Sciences, 62, 1175–1191, 2005.

Fernando, H., Princevac, M., Pardyjak, E., and Data, A.: The decay of convective turbulence during evening transition period, in: 11th Conference on Mountain Meteorology and MAP Meeting, Bartlett (NH), USA, paper 10.3, 2004.

Fitzjarrald, D. R., Freedman, J. M., Czikowsky, M. J., Sakai, R. K., and Moraes, O. L. L.: Momentum and scalar transport during the decay of CBL turbulence, 16th AMS Symposium on boundary layers and turbulence, 2004.

Gioli, B., Miglietta, M., Vaccari, F. P., Zaldei, A., and De Martino, B.: The Sky Arrow ERA, an innovative airborne platform to monitor mass, momentum and energy exchange of ecosystems, Annales Geophysicae, 49, 109–116, 2006.

Goulart, A., Degrazia, G., Rizza, U., and Anfossi, D.: A theoretical model for the study of convective turbulence decay and comparison with large-eddy simulation data, Boundary-Layer Meteorology, 107, 143–155, 2003.

Goulart, A., Bodmann, B., Vilhena, M., Soares, P., and Moreira, D.: On the Time Evolution of the Turbulent Kinetic Energy Spectrum for Decaying Turbulence in the Convective Boundary Layer, Boundary-Layer Meteorology, 138, 61–75, 10.1007/s10546-010-9546-4, 2010.

Grant, A. L. M.: An observational study of the evening transition boundary-layer, Quarterly Journal of the Royal Meteorological Society, 123, 657–677, 1997.

Grimsdell, A. W. and Angevine, W. M.: Observations of the afternoon transition of the convective boundary layer, Journal of Applied Meteorology, 41, 3–11, 2002.

Heo, B., Jacoby-Koaly, S., Kim, K., Campistron, B., Bénech, B., and Jung, E.: Use of the Doppler spectral width to improve the estimation of the convective boundary layer height from UHF wind profiler observations, Journal of Atmospheric and Oceanic Technology, 20, 408–424, 2003.

Hø jstrup, J.: Velocity spectra in the unstable planetary boundary layer, Journal of the Atmospheric Sciences, 39, 2239–2248, 1982.

Jacoby-Koaly, S., Campistron, B., Bernard, S., Bénech, B., Ardhuin-Girard, F., Dessens, J., Dupont, E., and Carissimo, B.: Turbulent dissipation rate in the boundary layer via uhf wind profiler doppler spectral width measurements, Boundary-Layer Meteorology, 103, 361–389, 2002.

Kaimal, J., Wyngaard, J., and Coté, O.: Spectral characteristics of surface layer turbulence, Quarterly Journal of the Royal Meteorological Society, 98, 653–689, 1972.

Kaimal, J., Wyngaard, J., Haugen, D., Coté, O., and Izumi, Y.: Turbulence structure in the convective boundary layer, Journal of the Atmospheric Sciences, 33, 2152–2169, 1976.

Kàrmàn, T.: Progress in the statistical theory of turbulence, Proc. Nat. Acad. Sci., 34, 530–539, 1948.

Kristensen, L. and Lenschow, D. H.: The spectral velocity tensor for homogeneous boundary-layer turbulence, Boundary-Layer Meteorology, 47, 149–193, 10.1177/1553350614532679, 1989.

Legain, D., Bousquet, O., Douffet, T., Tzanos, D., Moulin, E., Barrie, J., and Renard, J.-B.: High frequency boundary layer profiling with reusable radiosondes, Atmos. Meas. Tech. Discuss., 6, 3339–3365, 2013.

Lenschow, D. H. and Stankov, B. B.: Length scales in the convective boundary layer, Journal of the Atmospheric Sciences, 43, 1198–1209, 1986.

Lenschow, D. H., Mann, J., and Kristensen, L.: How Long is Long Enough When Measuring Fluxes and Other Turbulence Statistics?, Journal of Atmospheric and Oceanic Technology, 11, 661–673, 1994.

Lohou, F. and Patton, E. G.: Surface Energy Balance and Buoyancy Response to Shallow Cumulus Shading, Journal of the Atmospheric Sciences, 71, 665–682, 10.1175/JAS-D-13-0145.1, 2014.

Lohou, F., Saïd, F., Lothon, M., Durand, P., and Serça, D.: Impact of Boundary-Layer Processes on Near-Surface Turbulence Within the West African Monsoon, Boundary-Layer Meteorology, 136, 1–23, 10.1007/s10546-010-9493-0, 2010.

Lothon, M., Lenschow, D., and Mayor, S.: Coherence and Scale of Vertical Velocity in the Convective Boundary Layer from a Doppler Lidar, Boundary-Layer Meteorology, 121, 521–536, 10.1007/s10546-006-9077-1, 2006.

Lothon, M., Lenschow, D. H., and Schanot, A.: Status-reminder report on C-130 air-motion measurements. Test of DYCOMS-II new datasets, Internal report, NCAR-RAF, 2007.

Lothon, M., Lenschow, D., and Mayor, S.: Doppler Lidar Measurements of Vertical Velocity Spectra in the Convective Planetary Boundary Layer, Boundary-Layer Meteorology, 132, 205–226, 10.1007/s10546-009-9398-y, 2009.

Lothon, M., Lohou, F., Pino, D., Couvreux, F., Pardyjak, E. R., Reuder, J., Vilà-Guerau de Arellano, J., Durand, P., Hartogensis, O., Legain, D., Augustin, P., Gioli, B., Lenschow, D. H., Faloona, I., Yagüe, C., Alexander, D. C., Angevine, W. M., Bargain, E., Barrié, J., Bazile, E., Bezombes, Y., Blay-Carreras, E., van de Boer, A., Boichard, J. L., Bourdon, A., Butet, A., Campistron, B., de Coster, O., Cuxart, J., Dabas, A., Darbieu, C., Deboudt, K., Delbarre, H., Derrien, S., Flament, P., Fourmentin, M., Garai, A., Gibert, F., Graf, A., Groebner, J., Guichard, F., Jiménez, M. a., Jonassen, M., van den Kroonenberg, A., Magliulo, V., Martin, S., Martinez, D., Mastrorillo, L., Moene, a. F., Molinos, F., Moulin,

E., Pietersen, H. P., Piguet, B., Pique, E., Román-Cascón, C., Rufin-Soler, C., Saïd, F., Sastre-Marugán, M., Seity, Y., Steeneveld, G. J., Toscano, P., Traullé, O., Tzanos, D., Wacker, S., Wildmann, N., and Zaldei, A.: The BLLAST field experiment: Boundary-Layer Late Afternoon and Sunset Turbulence, Atmospheric Chemistry and Physics, 14, 10 931–10 960, 10.5194/acp-14-10931-2014, 2014.

Meneveau, C. and Katz, J.: Scale-Invariance and Turbulence Models for Large-Eddy Simulation, Annu. Rev. Fluid Mech., 32, 1–32, 2000.

Moeng, C. H.: A large-eddy-simulation model for the study of planetary boundary-layer turbulence, Journal of the Atmospheric Sciences, 41, 2052–2062, 1984.

Moeng, C.-H. and Wyngaard, J.: Spectral-analysis of large-eddy simulations of the convective boundary-layer, Journal of Atmospheric Sciences, 45, 3573–3587, 1988.

Monin, A. and Yaglom, A.: Statistical fluid mechanics, vol. 2, The MIT Press, Massachussets, 1975.

Nadeau, D., Pardyjak, E., Higgins, C., Fernando, H., and Parlange, M.: A Simple Model for the Afternoon and Early Evening Decay of Convective Turbulence Over Different Land Surfaces, Boundary-Layer Meteorology, 141, 301–324, 10.1007/s10546-011-9645-x, 2011.

Nieuwstadt, F. T. M. and Brost, R. A.: The decay of convective turbulence, Journal of the Atmospheric Sciences, 43, 532–546, 1986.

Patton, E. G., Sullivan, P. P., and Moeng, C. H.: The Influence of Idealized Heterogeneity on Wet and Dry Planetary Boundary Layers Coupled to the Land Surface, Journal of the Atmospheric Sciences, 62, 2078–2097, 2005.

Pietersen, H., Vilà-Guerau de Arellano, J., Augustin, P., Van de Boer, A., De Coster, O., Delbarre, H., Durand, P., Fourmentin, M., Gioli, B., Hartogensis, O., Lothon, M., Lohou, F., Ouwersloot, H., Pino, D., and Reuder, J.: Study of a prototypical convective boundary layer observed during BLLAST: contributions by large-scale forcing, Atmospheric Chemistry and Physics, 15, 4241–4257, 2015.

Pino, D., Jonker, H., Vilà-Guerau De Arellano, J., and Dosio, A.: Role of Shear and the Inversion Strength During Sunset Turbulence Over Land: Characteristic Length Scales, Boundary-Layer Meteorology, 121, 537–556, 10.1007/s10546-006-9080-6, 2006.

Rizza, U., Miglietta, M., Degrazia, G., Acevedo, O., and Marques Filho, E.: Sunset decay of the convective turbulence with Large-Eddy Simulation under realistic conditions, Physica A: Statistical Mechanics and its Applications, 392, 4481–4490, 10.1016/j.physa.2013.05.009, 2013a.

Rizza, U., Miglietta, M. M., Acevedo, O. C., Anabor, V., Degrazia, G. a., Goulart, A. G., and Zimmerman, H. R.: Large-eddy simulation of the planetary boundary layer under baroclinic conditions during daytime and sunset turbulence, Meteorological Applications, 20, 56–71, 10.1002/met.1284, 2013b.

Saïd, F., Corsmeier, U., Kalthoff, N., Kottmeier, C., Lothon, M., Wieser, a., Hofherr, T., and Perros, P.: ESCOMPTE experiment: intercomparison of four aircraft dynamical, thermodynamical, radiation and chemical measurements, Atmospheric Research, 74, 217–252, 10.1016/j.atmosres.2004.06.012, 2005.

Seity, Y., Brousseau, P., Malardel, S., Hello, G., Benard, P., Bouttier, F., Lac, C., and Masson, V.: The AROME-France Convective-Scale Operational Model, Monthly Weather Review, 139, 976–991, 2011.

Shaw, W. and Barnard, J.: Scales of turbulence decay from observations and direct numerical simulation, in: 15th Symposium on Boundary Layers and Turbulence, p. 8.3, Wageningen University, The Netherlands, 2002.

Sorbjan, Z.: Decay of convective turbulence revisited, Boundary-Layer Meteorology, 82, 501–515, 1997.

Sullivan, P., Mc Williams, J., and Moeng, C.-H.: A subgrid-scale model for large-eddy simulation of planetary boundary-layer flows, Boundary-Layer Meteorology, 71, 247–276, 1994.

Sullivan, P. P. and Patton, E. G.: The Effect of Mesh Resolution on Convective Boundary Layer Statistics and Structures Generated by Large-Eddy Simulation, Journal of the Atmospheric Sciences, 68, 2395–2415, 10.1175/JAS-D-10-05010.1, 2011.

Taylor, A., Beare, R., and Thomson, D.: Simulating Dispersion in the Evening-Transition Boundary Layer, Boundary-Layer Meteorology, 153, 389–407, 10.1007/s10546-014-9960-0, 2014.

Vilà-Guerau de Arellano, J., Dosio, A., Vinuesa, J.-F., Holtslag, a. a. M., and Galmarini, S.: The dispersion of chemically reactive species in the atmospheric boundary layer, Meteorology and Atmospheric Physics, 87, 23–38, 10.1007/s00703-003-0059-2, 2004.

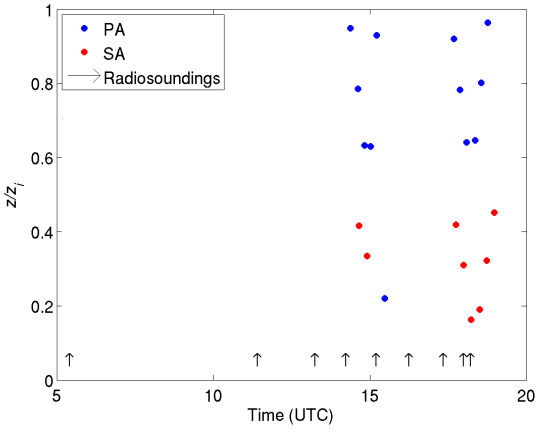

Fig. 1. Normalized altitude z/z_i (where z_i is the PBL depth) of the legs flown by the two aircraft the 20 June 2011 (Piper Aztec in blue, Sky Arrow in red) and launching times of the radiosoundings (black arrows).

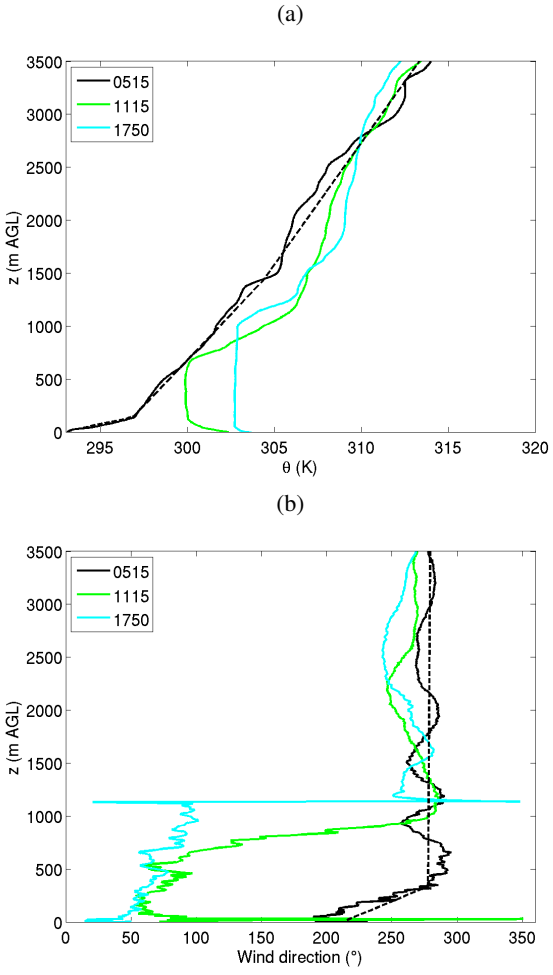

Fig. 2. Observed vertical profiles of (a) the potential temperature θ and (b) the wind direction on the 20 June 2011. The black dashed lines represent the initial profiles of the LES.

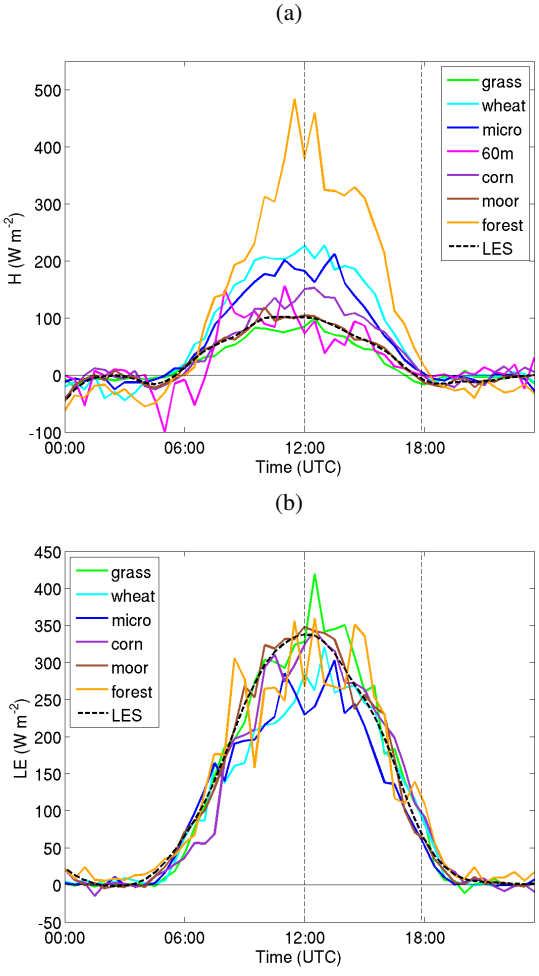

Fig. 3. Temporal evolution of (a) surface sensible (H) and (b) latent (LE) heat fluxes over several vegetation coverages, on 20 June 2011. Dashed black curves stand for the surface flux used as boundary conditions for the LES. The vertical dashed lines stand for the times of maximum surface buoyancy flux (at 1200 UTC) and zero value (at 1750 UTC).

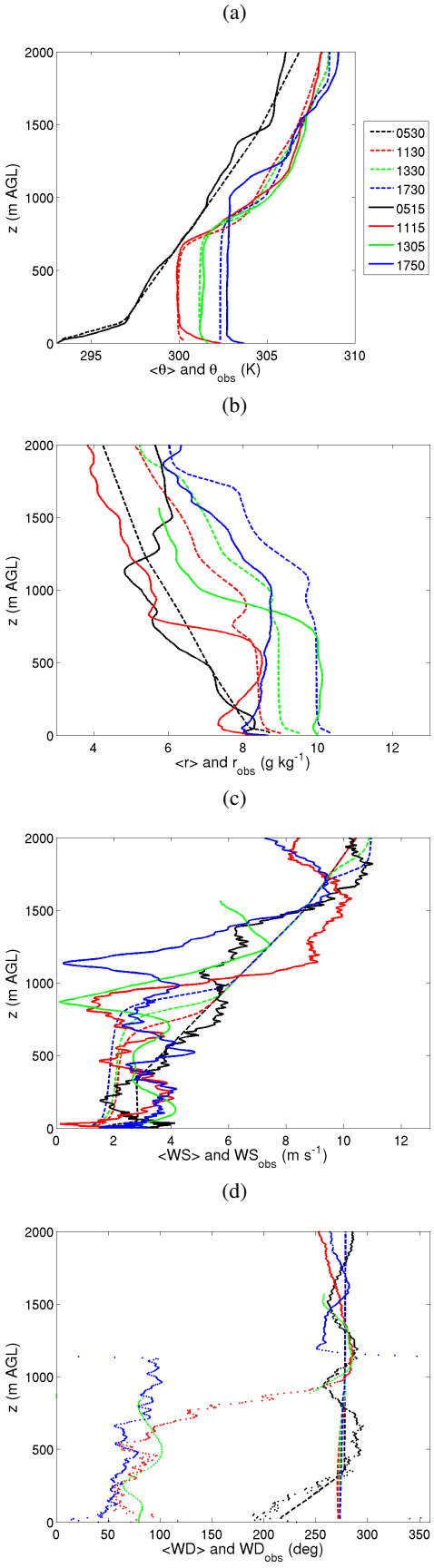

Fig. 4. Vertical profiles of (a) θ ,(b) r ,(c) wind speed (WS), (d) wind direction (WD) observed (solid lines and dotted lines for WD) and obtained by LES (dashed lines).

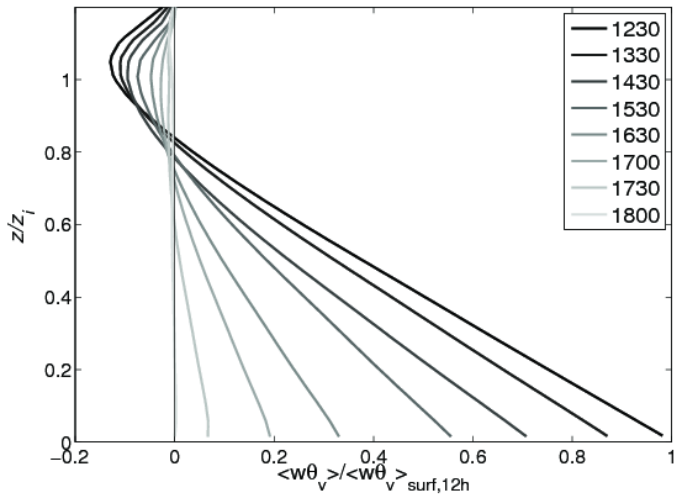

Fig. 5. Vertical profiles of the buoyancy flux normalized by the surface buoyancy flux at 1200 UTC according to the normalized height z/z_i.

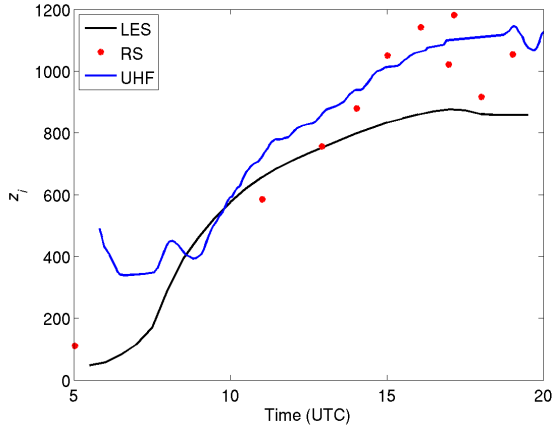

Fig. 6. Temporal evolution of z_i in the simulation (black), observed by the UHF wind profiler (blue) and depicted using radiosondes (RS) measurements (red dots).

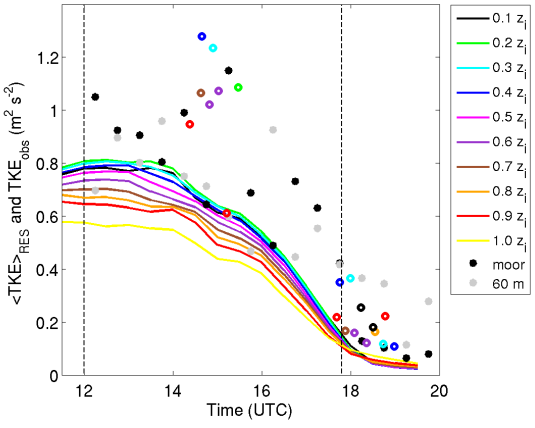

Fig. 7. Temporal evolution of the resolved TKE (subscript RES) at different heights in the simulation (different colors). TKE deduced from aircraft and surface (subscript OBS) spectra integrated over the LES spectra wavenumber range (open and filled circles, respectively). The vertical dashed lines stand for the times of maximum surface bouyancy flux (at 1200 UTC) and its zero value (at 1750 UTC).

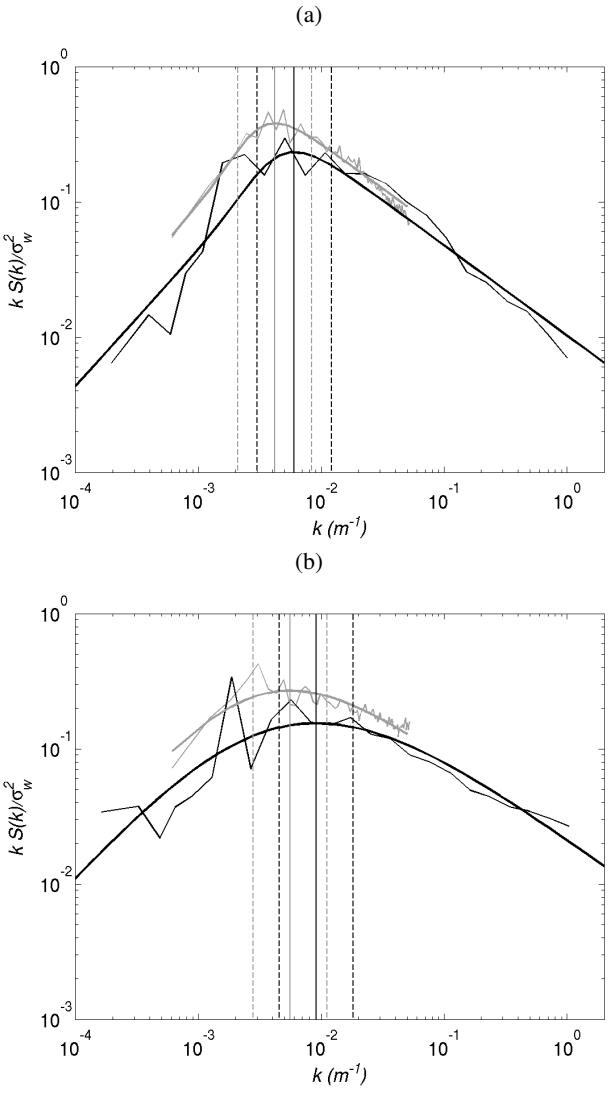

Fig. 8. Normalized w spectra at (a) 1500 and (b) 1800 UTC from both aircraft (black) and LES (grey), fitted with the $KL89$ analytical spectral model (thick lines). The vertical continous line represent Λ_w, the maximum energy wavenumber and the dashed vertical lines represent k_1 and k_2, the limits of the low wavenumber range and of the inertial subrange, defined as $k_1 = \pi/\Lambda_w$ and $k_2 = 4\pi/\Lambda_w$.

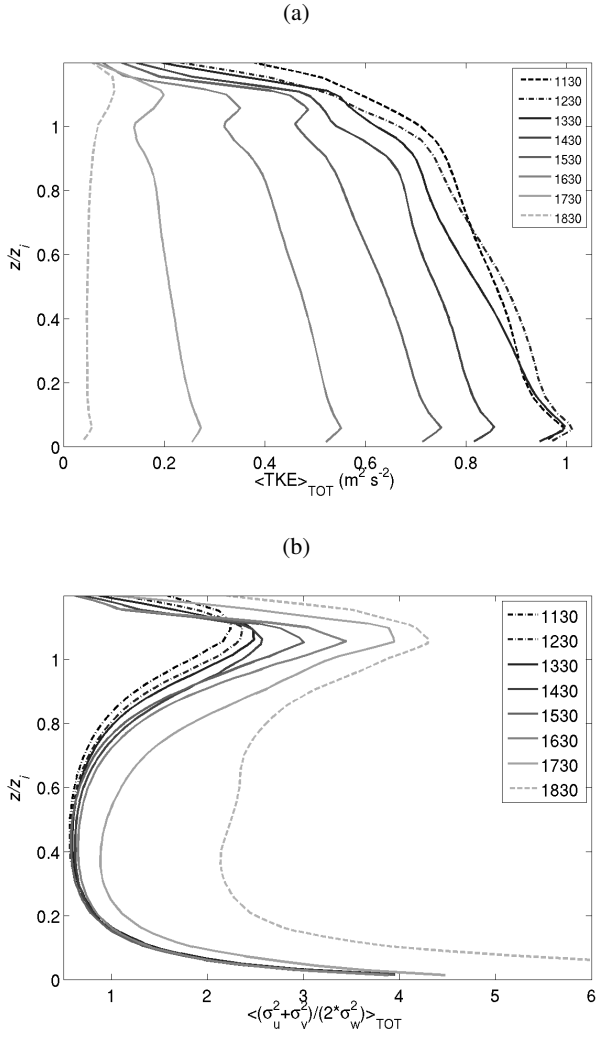

Fig. 9. Vertical profiles of the total (resolved and subgrid (subscript TOT)) (a) TKE and (b) anisotropy at several hours during the AT in the LES.

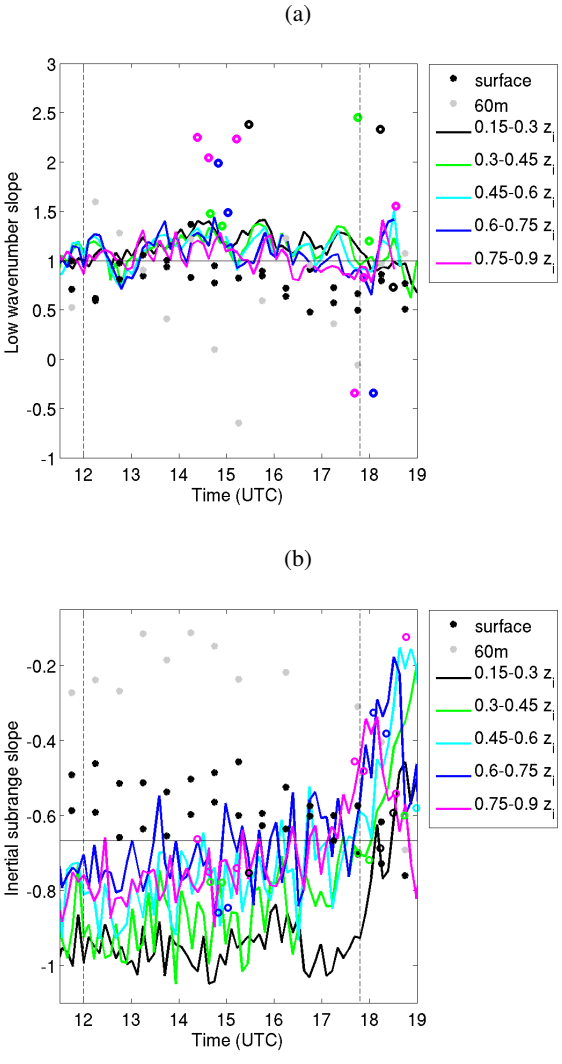

Fig. 10. Temporal evolution of the slopes in (a) the low wavenumber range and (b) the inertial subrange of the w spectra obtained by LES (continuous lines), aircraft and surface measurements (open and filled circles) at different heights (colors). The horizontal black lines stand for the theoretical expected values

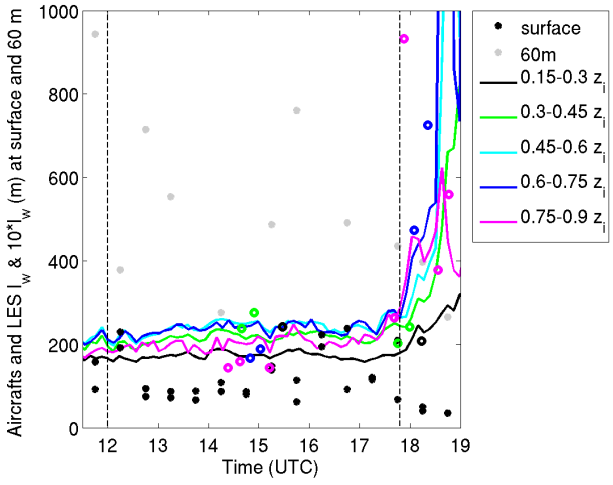

Fig. 11. Temporal evolution of l_w calculated from the $KL89$ analytical model fit on LES (continuous lines), aircraft (open circles) and surface (closed circles) spectra at different heights (different colors). Note that l_w at surface and at 60 m are multiplied by a factor 10. The vertical dashed lines stand for the times of maximum surface bouyancy flux (at 1200 UTC) and its zero value (at 1750 UTC).

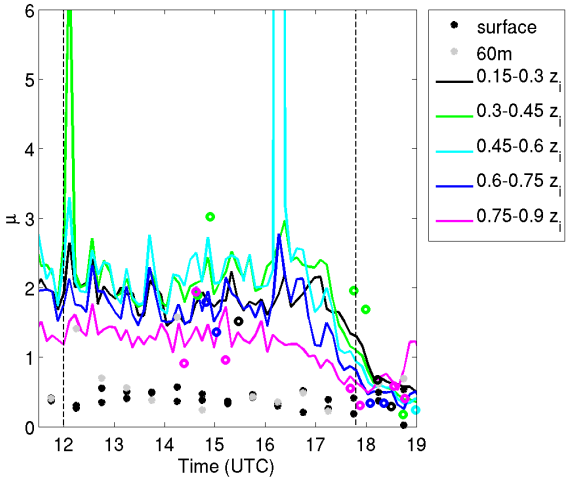

Fig. 12. Temporal evolution of the parameter μ, obtained from the $KL89$ analytical model, by using LES (continous lines), aircraft (open circles) and surface (closed circles) data. The vertical dashed lines stand for the times of maximum surface bouyancy flux (at 1200 UTC) and its zero value (at 1750 UTC).

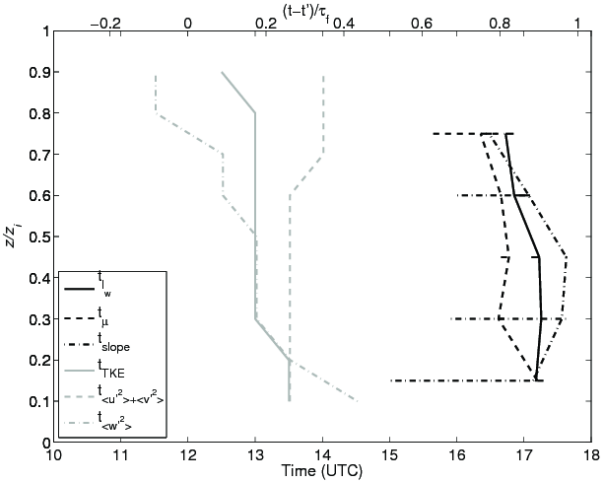

Fig. 13. Vertical profiles of the timings of changes observed in the evolution of the TKE, the vertical and horizontal variances, l_v, μ and the inertial subrange slope of w spectra. t' is defined as the time when H is maximum (i.e at 1200 UTC).